Angle Stability Analysis for Voltage-Controlled Converters

Lin, Hengwei; Jia, Chenxi; Guerrero, Josep M.; Quintero, Juan Carlos Vasquez

Published in:
I E E E Transactions on Industrial Electronics

DOI (link to publication from Publisher):
10.1109/TIE.2017.2682022

Publication date:
2017

Document Version
Early version, also known as pre-print

Angle Stability Analysis for Voltage-Controlled Converters

Hengwei Lin, *Member, IEEE*, Chenxi Jia, *Student Member, IEEE*,
Josep M. Guerrero, *Fellow, IEEE*, Juan C. Vasquez, *Senior Member, IEEE*

***Abstract*—Power electronics based voltage source converters (VSCs) keep increasing in modern electrical systems. As a branch of stability problems, angle stability is significant for an electrical system. Based on small disturbance analysis and time scale decomposition perspective, this paper proposes a criterion to analyze the quasi-steady angle stability and the direct current (DC) side stability for VSCs. The operating limit and the angle instability mechanism are revealed, which is generally applicable to the voltage-controlled converters. During the analysis, the influence of the parameters on angle stability is studied. Further, the difference on instability mechanism between power electronic converters and synchronous generators are explained in detail. Finally, experiment results with corrective actions verify the analysis.**

***Index Terms*—Angle stability, damping, equivalent circuit, eigenvalue, frequency domain analysis, output impedance, operating limit, quasi-steady state, small disturbance analysis, steady state, time domain analysis, time scale decomposition.**

I. INTRODUCTION

VOLTAGE source converters (VSCs) have been widely used in electrical system, such as the motor drives, flexible alternating current transmission systems (FACTS), high voltage direct current (HVDC) transmission systems and renewable energy systems. VSC has the advantage on voltage/reactive power support, black-start capability and the possibility to connect to weak systems. The grid-tied converters worked in voltage-controlled mode (VCM) have the above superior features that are considered to build the future power systems as static synchronous generators.

As one of the key components in modern power systems, grid-connected converters influence the stability of the system significantly. In the previous literatures, the grid-connected inverters are usually controlled as current source with a current feedback controller or as power source using both current and power controllers. The design of the current regulator is introduced in [1]-[3], which show that the performance of the converters is determined by the control frame, dc bus voltage and sampling delays. The instability of grid-connected converters was studied by using negative incremental resistance concept in [4]-[8]. In current-controlled mode (CCM), phase-locked loop (PLL) is often used to obtain an accurate synchronization to the power grid. In [9]-[11], the effect of PLL was introduced. The investigations reveal that high bandwidth of PLL decreases the stability of VSCs since it increases the negative real part of the output impedance. Virtual impedance is proposed for VSCs to improve the system damping and mitigate the harmonic instability [12]-[14]. The impedance-based analysis methodology for current-controlled converters is discussed in [15]-[17]. Meanwhile, Nyquist stability criterion is applied to the return-ratio matrix between the load impedance and source impedance. Though the performance of current-controlled converters is attractive, one of the drawbacks of CCM converters is that they can not work in stand-alone mode independently. It can only work well based on the support from voltage sources, whilst influencing the system.

Compared with CCM, the converters that are operated in VCM have the advantage to support/control the voltage profile and frequency in the network. This critical feature is preferred in HVDC systems and renewable energy based systems. A simple voltage control scheme for converters usually contains an inner current loop with a voltage feedback loop keeping voltage constant. For parallel grid-connected inverters, there is often a power droop control loop beyond the voltage loop regulating the output power. Several control schemes as VCM are proposed [18]-[20]. The stability dependent on eigenvalue analysis is discussed for droop control in [21]-[22].To enhance the damping and power sharing capability, virtual impedance is proposed to shape the dynamic profiles [23]-[25]. The main advantage of the impedance based approach is that both the control and physical components are considered in the model. This method is also widely used in DC electrical systems [26].

In the recent years, some literatures are introducing to imitate synchronous generators for VSCs to improve the stability. Some control strategies named synchronverter [27], virtual synchronous generators [28]-[29] or virtual synchronous machines [30] are proposed. The above methods are all based

Manuscript received July 30, 2016; revised January 9, 2017; accepted February 13, 2017.

Hengwei Lin, Josep M. Guerrero and Juan C. Vasquez are with the Department of Energy Technology, Aalborg University, Aalborg 9220, Denmark (e-mail: hwe@et.aau.dk; joz@et.aau.dk; juq@et.aau.dk).

Chenxi Jia is with the Department of Electrical Engineering, Beijing Jiaotong University, Beijing, China (e-mail: mobolo@163.com).

Color versions of one or more of the figures in this paper are available online at http://ieeexplore.ieee.org.

Digital Object Identifier

on the idea of virtual inertia and DC-link storage to mimic the synchronous generators in the electrical system. However, there are few literatures to intrinsically reveal the angle instability mechanism of VSCs which may finally answer the question whether and which kind of VSCs has the ability to replace synchronous generators to support the power system. Angle stability is usually regarded as short-term problem (last typically several seconds following a disturbance) in traditional electrical systems and is usually related to the kinetic inertia of generators [31]-[32]. Therefore, it is important to study the angle stability and the corresponding criterion for VSCs.

The aim of this paper is to overcome the aforementioned drawbacks and to reveal the angle instability mechanism of VCM inverters. Through the mathematical deduction, the difference between VSCs and synchronous generators is expounded. The paper is organized as fellows: The equivalent circuit and the output impedance of VCM inverters are presented with frequency domain method in Section II. In order to reveal the instability mechanism and evolution, Section III proposes the system model based on time scale decomposition perspective. The stability criteria and instability mechanism is given in this part. The stability of DC side is analyzed in section IV. In Section V, the experiment verification with the corrective actions is presented. Section VI concludes the paper.

II. VOLTAGE CONTROL THEORY FOR POWER ELECTRONIC CONVERTERS

A. General Voltage Control Scheme for VSC

Fig. 1 shows the control system for voltage-controlled inverters. In this case, the LCL filtered VSC is controlled as a voltage source. The output voltage of VSC can be regulated by the voltage controller, while the inner current loop improves the transient performance. The vector of the output voltage $\dot{V}_o$ and the grid voltage $\dot{E}$ at the point of common coupling (PCC) are given by:

$$\dot{V}_o = \frac{2}{3}(v_a + e^{j\frac{2\pi}{3}} v_b + e^{j\frac{4\pi}{3}} v_c) \tag{1}$$

$$\dot{E} = \frac{2}{3}(e_a + e^{j\frac{2\pi}{3}} e_b + e^{j\frac{4\pi}{3}} e_c) \tag{2}$$

where

$$v_a = V_o \cos(\omega t + \delta)$$
$$v_b = V_o \cos(\omega t - \frac{2}{3}\pi + \delta)$$
$$v_c = V_o \cos(\omega t - \frac{4}{3}\pi + \delta)$$
$$e_a = E \cos(\omega t)$$
$$e_b = E \cos(\omega t - \frac{2}{3}\pi)$$
$$e_c = E \cos(\omega t - \frac{4}{3}\pi)$$

ω is the angular synchronous frequency of the alternating current (AC) source. The dynamic equation of the converter is

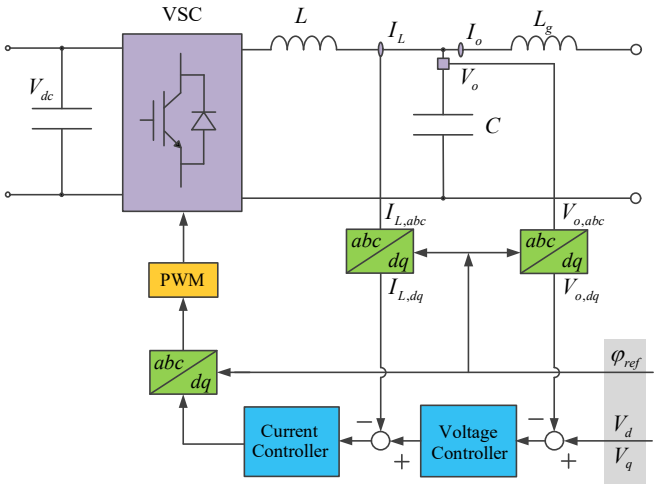

Fig. 1. Single phase diagram of the voltage-controlled VSC.

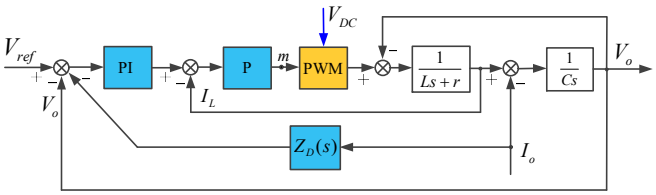

Fig. 2. Block diagram of the voltage and current control loop.

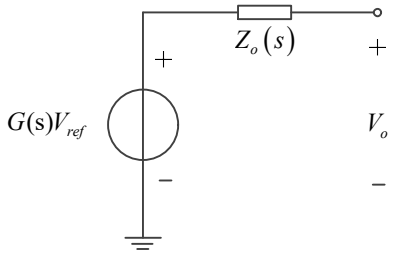

Fig. 3. The equivalent circuit of the voltage-controlled VSC.

presented as following:

$$L\frac{dI_L}{dt} = mK_m - V_o - rI_L \tag{3}$$

$$C\frac{dV_o}{dt} = I_L - I_o \tag{4}$$

where r is the parasitic resistance of the inductor L. m is the modulating (reference) signals for pulse width modulation (PWM). V_{dc} is the DC side voltage that is assumed as a constant in this section. K_m is the transfer gain of VSC's half-bridge circuit which has $K_m=V_{dc}/(2V_{tri})$. V_{tri} is the amplitude of the PWM wave and usually set as 1. When the DC side voltage V_{dc} is constant, K_m keeps constant and the DC-link can be regarded decoupled with the AC side. The component K_m is significant for the DC side stability analysis in Section IV. (For more details, please refer to modulation theory.)

For convenient engineering design and analysis, the block diagram of the control system in frequency domain is illustrated

in Fig. 2. In the control loop, there is an additional virtual impedance controller $Z_D(s)$ shaping the output impedance of VSC to against the disturbance from the output current. s is the Laplace operator. The voltage controller is a proportion and integrator (PI) $k_p+k_i\frac{1}{s}$, while the inner current controller is a proportion (P) k. The adopted current controller (P or PI) does not influence the final mathematical deduction in Section IV. According to Mason's formula, the transfer function of VSC with the closed loop control can be expressed as following:

$$V_o = G(s)V_{ref} - Z_o(s)I_o \tag{5}$$

where the voltage gain $G(s)$ and the current (disturbance) gain $Z_o(s)$ are given below:

$$G(s) = \frac{K_m k k_p s + K_m k k_i}{LCs^3 + (r + K_m k)Cs^2 + (K_m k k_p + 1)s + K_m k k_i} \tag{6}$$

$$Z_o(s) = \frac{Ls^2 + (r + K_m k + K_m k k_p Z_D(s))s + K_m k k_i Z_D(s)}{LCs^3 + (K_m k + r)Cs^2 + (K_m k k_p + 1)s + K_m k k_i} \tag{7}$$

From equation (5), the voltage-controlled VSC can be modelled as a two terminal Thevenin equivalent circuit that is shown in Fig. 3. The controlled voltage source is $G(s)V_{ref}$ while the series output impedance is $Z_o(s)$. Since the virtual impedance $Z_D(s)$ does not exist in the voltage gain $G(s)$, it is often controlled flexibly to improve the performance of VSCs [24]-[25].

B. The Outer Loop Controller for VSC

For grid-connected inverter, there is often a power control loop beyond the inner voltage and current control regulating the active/reactive power, as is shown in Fig. 4. The inner controller can be adopted as is given in Fig. 1.

In power system, the network is mainly inductive so the P-ω and Q-V scheme is adopted. The voltage frequency and magnitude of the inverter can be controlled as:

$$\omega = \omega^* - (k_{p\omega} + k_{i\omega}\frac{1}{s})(P - P^*) \tag{8}$$

$$V = V^* - (k_{pv} + k_{iv}\frac{1}{s})(Q - Q^*) \tag{9}$$

$$V_{ref} = V \cdot \sin \omega t \tag{10}$$

where $k_{p\omega}+k_{i\omega}\frac{1}{s}$ and $k_{pv}+k_{iv}\frac{1}{s}$ are the active power and reactive power controller respectively.

Fig. 5 gives the diagram of another voltage control strategy with a PLL loop that is also widely used in electrical systems. Comparing Fig. 4 and Fig. 5, it can be found that PLL plays as an outer loop similarly as the power control loop such that PLL should have a relative low bandwidth to avoid unnecessary instable. As the green blocks shown in Fig. 1, Fig. 4 and Fig. 5, there are inherent nonlinear functions in VSCs, regardless of the adopted control frame (*d*-*q*, *abc* or *α*-*β*). Since these nonlinear functions are often neglected, the previous stability analyses for VSCs usually perform separately dd, dq, qd, and qq axles.

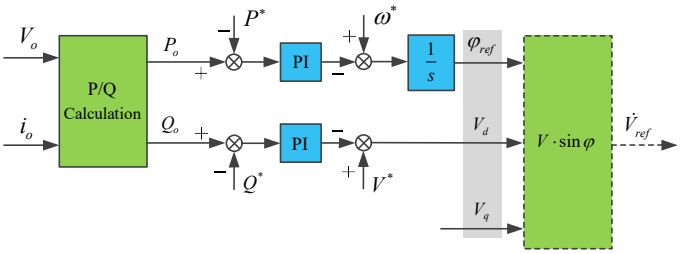

Fig. 4. Block diagram of power control loop.

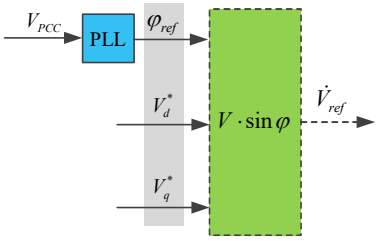

Fig. 5. Block diagram of voltage-controlled scheme with PLL as the outer loop.

Without losing representativeness, the following part in this section mainly discusses the power control as the outer loop for voltage-controlled VSCs. Owing to the multiply operators both for calculating the output power (P_o and Q_o) and the final resultant reference, the power control is a typical multi-input nonlinear closed control loop (Fig. 4). The previous literatures often treat this control loop as linear and (or) open loop, which may influence the conclusion or accuracy in some specific cases. Meanwhile, the power loop brings an additional output impedance $Z_p(s)$ that is related to the output current/power rating. The active power controller mainly influences the phase of the output impedance $Z_p(s)$ (in a nonlinear way), while the reactive power controller influences the magnitude of $Z_p(s)$. The final output impedance of VSCs in frequency domain can be expressed as:

$$Z(s) = Z_o(s) + Z_p(s) \tag{11}$$

To simplify the analysis, [23] assumes the output impedance of VSCs is mainly influenced by inner voltage loop $Z_o(s)$. This assumption is reasonable if virtual impedance is added in the inner control loop to improve the system's damping to against the disturbance from I_o. The bode diagram of the output impedance is shown in Fig. 6 and Fig. 7. The parameters here are given in Table I. It can be found that the virtual impedance can influence the characteristics of the total output impedance in its limited bandwidth.

However, in order to generally reveal the angle stability of the voltage-controlled VSCs, the following stability deduction in this paper is based on the algebraic expression. For the time domain analysis in the next section, the actual output impedance Z of VSC can be easily transformed from frequency domain into time domain:

$$Z(j\omega) = R_z + jI_z \tag{12}$$

where R_z is the real part of Z and I_z is the imaginary part.

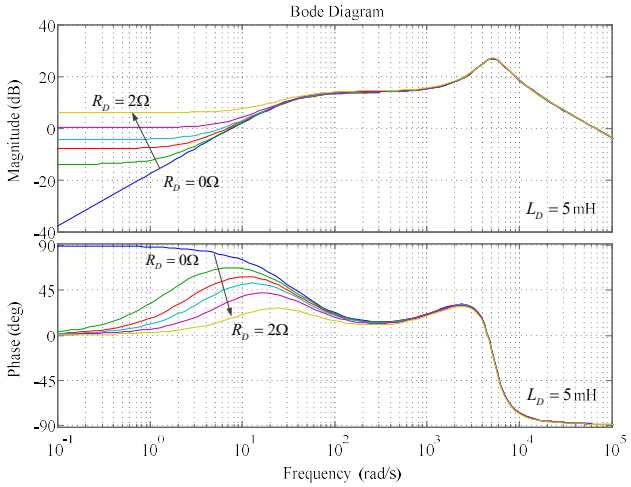

Fig. 6. Bode diagram of output impedance with increasing virtual resistance.

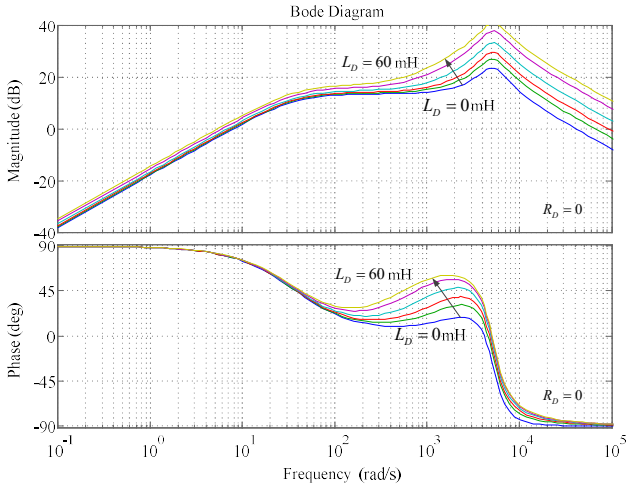

Fig. 7. Bode diagram of output impedance with increasing virtual inductance.

TABLE I
THE PARAMETERS IN CONTROL SYSTEM AND VSC

Parameters	Description	Value
f_s	PWM switching frequency	10kHz
V_{dc}	DC side voltage source	650V(10kW)
V^*	Voltage reference	311V
k	Proportional term in current loop	5.65
k_p	Proportional term in voltage loop	0.04
k_i	Integral term in voltage loop	8
k_{pv}	Proportional term in reactive power loop	0.003
k_{iv}	Integral term in reactive power loop	0
$k_{p\omega}$	Proportional term in active power loop	0.001
$k_{i\omega}$	Integral term in active power loop	0
ω_c	The cut-off frequency of low pass filter	60
L	The filter inductance at converter side	1.8mH
r	Parasitic resistance in filter inductance	0.1Ω
C	Filter capacitance	25μF
L_g	The filter inductance at grid side (regarded as the line impedance)	1.8mH
R_D	Virtual resistance	0.5Ω
L_D	Virtual inductance	5mH
R_{Load}	Resistive load	57Ω

When ignoring the influence of the outer power control loop, the nonlinear output impedance of the inner control loop $Z_o(s)$ is given below:

$$R_z = \frac{A_1}{B}$$

$$I_z = \frac{A_2}{B}$$

where the expression of A_1, A_2 and B are given in the appendix, respectively.

III. ANGLE STABILITY ANALYSIS FOR VSC

A. Time Scale Decomposition Perspective

Time domain analysis has the advantage of actually revealing the evolution of a dynamical system. The small disturbance analysis of an electrical system can be described as a group of differential-algebraic (DA) equations:

$$\dot{z} = h(z, x, y) \tag{13}$$

$$\dot{x} = f(z, x, y) \tag{14}$$

$$0 = g(z, x, y) \tag{15}$$

where z is the long-term and mid-term state variables, x is the short-term and transient variables and y is the algebraic variables respectively.

In stability analysis, the network is assumed instantaneous response such that the network is described by the algebraic equations [33], including y of the voltage magnitudes and phase angles. The short-term and transient dynamics x last typically for several seconds at most following a disturbance, while the mid-term and long-term component z (may contain discrete dynamics) acts typically in minutes. When a disturbance occurs, the short-term dynamics exist first and decay rapidly, but the slow dynamics do not response yet. Once the system survived from the short-term response in a disturbance, it begins to be driven by mid- and long-term variables. The theoretical stability analysis of a dynamical system is given in subsection 2 of the appendix for further reading.

For power electronics based VSCs, however, the dynamics of the controller are extremely fast due to the PWM frequency whose action cycle is often above 10 kHz. Since the controller has been studied and plays well with appropriate Bode or Nyquist diagram design, this paper assumes the controller's dynamics infinitely fast and the system survived from the transient dynamics of the controller in a disturbance, which reserves and focus on the other dynamics. In this condition, as the quasi-steady state approach, the transient dynamics of VSCs can be replaced with equilibrium:

$$\dot{z} = h(z, x, y) \tag{16}$$

$$0 = f(z, x, y) \tag{17}$$

$$0 = g(z, x, y) \tag{18}$$

B. Active Power versus Angle Stability

Based on the above perspective and circuit theory, Fig. 8 gives the equivalent circuit of a voltage-controlled inverter connected to the power grid. $V^*\angle\varphi$ is the given voltage reference, $V_o\angle\delta$ is the output voltage, $E\angle 0$ is the grid voltage and $Z_L\angle\theta = R + jX$ is the line impedance. Z is the equivalent output impedance of VSC, which is calculated in Section II.

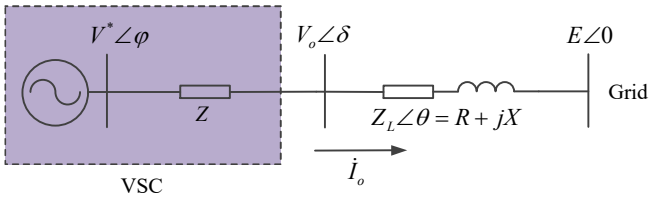

Fig. 8. Equivalent circuit of an inverter connected to power grid.

The output complex power drawn to the grid can be expressed as below:

$$S = \dot{V}_o \dot{I}_o^* \tag{19}$$

$$\dot{I}_o = \frac{\dot{V}_o - \dot{E}}{R + jX} \tag{20}$$

$$\dot{V}_o = \dot{V}^* - Z\dot{I}_o \tag{21}$$

Substituting the equations (20), (21) into (19), we can get:

$$P = \frac{V^*V_oR\cos\varphi - V^*V_oX\sin\varphi + 2R_zEV_o}{R^2+X^2}\cos\delta - \frac{R_z\left(V_o^2+E^2\right)}{R^2+X^2} + \frac{V^*V_oX\cos\varphi + V^*V_oR\sin\varphi}{R^2+X^2}\sin\delta - \frac{V^*ER\cos\varphi}{R^2+X^2} + \frac{V^*EX\sin\varphi}{R^2+X^2} \tag{22}$$

$$Q = \frac{V^*V_oX\cos\varphi + V^*V_oR\sin\varphi + 2EV_oI_z}{R^2+X^2}\cos\delta - \frac{I_z\left(V_o^2+E^2\right)}{R^2+X^2} + \frac{V^*V_oX\sin\varphi - V^*V_oR\cos\varphi}{R^2+X^2}\sin\delta - \frac{V^*EX\cos\varphi}{R^2+X^2} - \frac{V^*ER\sin\varphi}{R^2+X^2} \tag{23}$$

The sensitivity of the output active power P to the operating voltage angle δ can be obtained through taking partial differential on (22) with δ:

$$\frac{\partial P}{\partial\delta} = \sin(\mu-\delta)\sqrt{\left(\frac{\left(V^*V_oR\cos\varphi - V^*V_oX\sin\varphi + 2R_zEV_o\right)}{R^2+X^2}\right)^2 + \left(\frac{\left(V^*V_oX\cos\varphi + V^*V_oR\sin\varphi\right)}{R^2+X^2}\right)^2} \tag{24}$$

where

$$\mu = \arctan\frac{Z_LV^*\sin(\varphi+\theta)}{Z_LV^*\cos(\varphi+\theta) + 2R_zE} \tag{25}$$

When $\frac{\partial P}{\partial\delta}>0$, which equals to $0<\delta<\mu$, the system is operated as negative feedback control and keeps angle stable:

$$\frac{\partial P}{\partial\delta} > 0 \tag{26}$$

The maximum operating limit of δ equals to μ, which is the singularity-introduced bifurcation:

$$\delta_{\max} = \arctan\frac{Z_LV^*\sin(\varphi+\theta)}{Z_LV^*\cos(\varphi+\theta) + 2R_zE} \tag{27}$$

C. Maximum Operating Angle Difference

The P-δ curve is given in Fig. 9, while curve 1 is the ideal operating characteristic without output impedance. It can be observed that the output active power is the function of the angle difference δ between VSC and the grid reference point. There are two operating points **a** and **b** corresponding to the

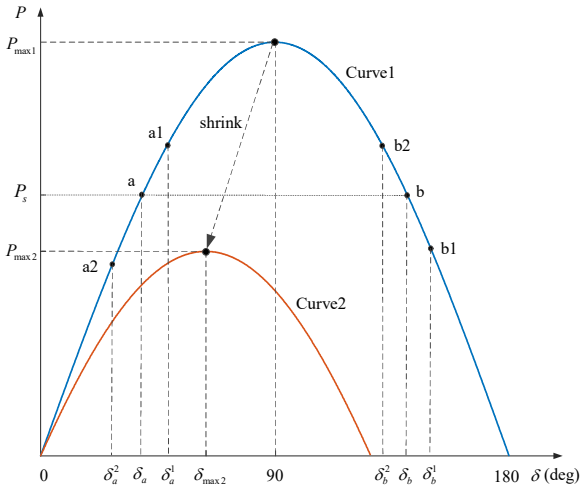

Fig. 9. The P-δ characteristic curve.

output active power P_s, but **a** is the stable operating point. Assume there is a small positive disturbance $\Delta\delta$ imposed on δ_a so that the power angle increases to δ_a^1. In this case, P_s becomes larger and makes the output power decrease according to the negative feedback control. It finally leads to the power angle decreases back to δ_a. Since the DC voltage is assumed constant, it can be regarded as no influence from/on DC side. For synchronous generators, this small disturbance leads to the rotor accelerate/decelerate and finally makes the electrical angle come back to δ_a. The dynamic process of the mechanical generators is mainly depending on the rotational inertia (rotational kinetic energy) while VSC is depending on the control schemes. This feature leads to the transient response of VSCs is superior to generators. Due to the inertia, there are inevitable swings on the rotor of a generator in a disturbance. On the other hand, for operating point **b** ($\left(\frac{\partial P}{\partial\delta}\right|_{\delta_b}$ <0), the behavior of the system changes inversely (positive feedback control) such that the system loses stability.

Equation (27) shows that the maximum angle is related to the voltage reference, the output impedance as well as the line impedance. $\delta_{\max}$ is the decreasing function of the real component R_z of VSC output impedance. When $0<\varphi+\theta<90°$ and $R_z>0$, $\delta_{\max}$ is the increasing function of line impedance Z_L and the voltage reference $V^*\angle\varphi$ (both the magnitude and phase). The previous literatures often ignore the influence of the given reference in VSCs during the stability analysis.

Normally, the inverter reference is set as unit power factor (φ=0). Equation (27) can be simplified as:

$$\delta_{\max} = \arctan\frac{XV^*}{RV^* + 2R_zE} \tag{28}$$

From (28), it can be found $\delta_{\max}$ is the decreasing function of R and increasing function of X. In a mainly inductive network, the line resistance can be ignored further. We have:

$$\delta_{\max} = \arctan\frac{XV^*}{2R_zE} \tag{29}$$

If $R_z\approx 0$ for VSC, $\delta_{\max}\approx 90°$. As the controller has significant influence on the output impedance Z, the operating

limit may decrease. As can be seen in Fig. 9, the maximum deliverable active power $P_{\max}$ and angle $\delta_{\max}$ (of curve 2) decrease when R_z (or R) increases. If the system operating curve shrinks from curve 1 to curve 2, the system may lose equilibrium for a constant power consumption P_s so as to be instable.

Come back to equation (27) and assume the equilibrium exists. In islanded mode or distribution system, the line impedance is relative small and we can assume X=R. At this situation, the maximum operating angle will be less than 45° with the grid angle reference is 0°. As the output impedance of VSC increases, the operating margin decreases further. For uninterrupted power supply (UPS) systems, the limit may be much less due to the small values of X and R and non-ignorable Z. When the system walks close to the edge paradigm, everything fails suddenly. The system should have a "safety margin" to avoid the catastrophe of a free fall. In critical condition, increasing the magnitude of voltage reference is helpful to increase the operating margin. It can be easily known that a higher voltage source allows a higher power delivered to the load.

IV. DC Side Influence on the System Stability

A. Constant DC Input Power

The above analysis is based on the assumption of constant DC voltage, this part we consider another condition: constant DC input power. Though the DC-link is often controlled constant for two-stage VSCs, the operating mode may become to constant DC input power under a disturbance or fault. In this case, K_m is inconstant, so that the VSC's output power S is the function of V_{dc}. The charging state (i_{in}=i_c+i_s) of DC-link is shown in Fig. 10. Assume V_{dc}^o is the current operating point on DC side and δ^o is the operating voltage angle on AC side. The charging current of the capacitor on DC-link is given below:

$$i_c = C_{dc}\frac{dV_{dc}}{dt} \tag{30}$$

Based on the law of energy conservation, the dynamic equation of DC side can be expressed as:

$$\frac{dV_{dc}}{dt} = \frac{P_{in}-P_{out}}{C_{dc}V_{dc}} \tag{31}$$

where P_{in} and P_{out} are the power flows through in and out the DC-link. The partial derivative of (31) at operating point V_{dc}^o is given in (32).

$$J(V_{dc}^o) = -\frac{1}{C_{dc}V_{dc}^{o^2}}\left[\left.\frac{\partial P_{out}}{\partial V_{dc}}\right|_{V_{dc}^o}\cdot V_{dc}^o + \left(P_{in}-P_{out}\big|_{V_{dc}^o}\right)\right] \tag{32}$$

When (32) has negative real part, the operating point is stable:

$$\mathrm{Re}\left\{-\frac{1}{C_{dc}V_{dc}^{o^2}}\left[\left.\frac{\partial P_{out}}{\partial V_{dc}}\right|_{V_{dc}^o}\cdot V_{dc}^o + \left(P_{in}-P_{out}\big|_{V_{dc}^o}\right)\right]\right\} < 0 \tag{33}$$

Simplify the above equation:

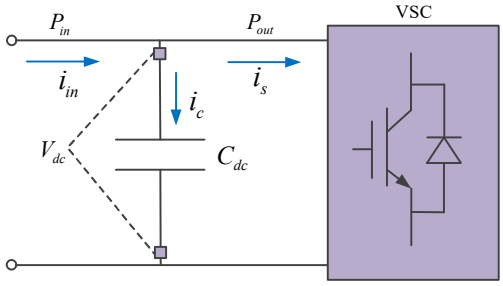

Fig. 10. The charging state of DC-link side.

$$\left.\frac{\partial \mathrm{Re}(P_{out})}{\partial V_{dc}}\right|_{V_{dc}^o}\cdot V_{dc}^o + P_{in} - \mathrm{Re}(P_{out})\big|_{V_{dc}^o} > 0 \tag{34}$$

When there is no loss on VSC, we can assume the VSC's output complex power S=P_{out}, namely Re(P_{out})=P. Then:

$$\left.\frac{\partial P}{\partial V_{dc}}\right|_{V_{dc}^o}\cdot V_{dc}^o + P_{in} - P\big|_{V_{dc}^o} > 0 \tag{35}$$

where the output active power P in (22) can be simplified by eliminating $V_o\angle\delta$:

$$\begin{aligned} P = {} & \frac{\left(V^{*2}-EV^*\cos\varphi\right)(R_z+R)+EV^*\sin\varphi(I_z+X)}{(R_z+R)^2+(I_z+X)^2} \\ & -R_z\frac{V^{*2}+E^2+2EV^*\cos\varphi}{(R_z+R)^2+(I_z+X)^2} \end{aligned} \tag{36}$$

The equation (35) and (36) can be solved once the parameters of the system are known, while R_z and I_z contain the influence of the control system (as is given in the appendix). For discharging state (i_{in}=i_s-i_c), the direction of i_c is reverse with (30) so that the final criteria is the same with (35). Therefore, the final criteria of the quasi-steady angle stability in case of constant DC input power, equations (35), (26) must be satisfied simultaneously. Rewrite them as following:

$$\begin{cases} \left.\dfrac{\partial P}{\partial V_{dc}}\right|_{V_{dc}^o}\cdot V_{dc}^o + P_{in} - P\big|_{V_{dc}^o} > 0 \\ \left.\dfrac{\partial P}{\partial \delta}\right|_{\delta^o} > 0 \end{cases} \tag{37}$$

Actually, (37) contains the eigenvalues (of Jacobian) in (16) - (18) for VSC angle stability that linearized around the system operating point V_{dc}^o,δ^o. The proposed methodology is reasonable for small disturbance analysis when PWM and the controller are very fast. From the above deduction, it can be found that both the DC side and the P-δ characteristic influence the angle stability. The criterion on DC side mainly ensures the stability of transferring enough energy to AC side, while the P-δ characteristic of AC network ensures the sensitivity is nonsingular and the control system is operated as negative feedback control. Since the above analysis is based on algebraic expression, it is generally appropriate for the voltage-controlled VSCs that can be indicated in Fig. 8. After appropriate engineering design for the controllers (bandwidth, margin and damping) in VSCs, (27)-(29) can be easily used to estimate the angle margin for the current operating state.

B. Comparison with Synchronous Generators

The above criteria deduction is different with synchronous generators, since there are only electrical/electromagnetic variables in VSCs. For comparison, the dynamic equation (in per unit) of the rotor in synchronous generators is given below:

$$T_J \frac{d^2\delta}{dt^2} = P_m - P_E \tag{38}$$

where P_m is the input mechanical power and P_E is the output electric power. $T_J = \frac{J\Omega_N^2}{S_N} = 2\text{H}$ is a constant. H is the inertia constant (MJ/MVA or MW·s/MVA). J is rotor moment of inertia ($\text{kg}\cdot\text{m}^2$). Ω_N and S_N are the synchronous angular velocity (rad/s) and the rated capacity of the generator, respectively.

Due to the inertia and the response of speed regulator, the input mechanical power is often assumed constant for synchronous generators. In this case, the angle stability criterion for (38) is:

$$\frac{\partial P_E}{\partial \delta} > 0 \tag{39}$$

It can be observed that the criterion for angle stability is the same with (26). Since there are only electrical variables in VSCs, the response of VSCs can be much faster than mechanical generators e.g. storage based VSCs. When the DC side ensures the stability to transfer enough primary energy, VSCs have the ability to replace the synchronous generators with stable operation and fast transient response (and of course different control schemes).

V. Experiment with Corrective Actions

A. Experiment Illustration and Analysis

In this Section, we utilize experiments with several corrective actions to illustrate the validity of the above analysis. Since the exact parameters of the power grid are difficult to estimate, the experiment is performed on two parallel VSCs with a resistive load consuming the output active power. The diagram of the experiment system is shown in Fig. 11, while the parameters in *d-q* frame are given in Table I. In the test, the LCL inductance filter at grid side L_g is regarded as the line impedance. The voltage references of VSCs are set as unit factor here. According to (28), the line resistance can decrease the operating margin similarly as the virtual resistance of VSCs. Because it is difficult to continuously change the line impedance in the experiment, we illustrate the influence of VSC's output impedance in the paper.

In Fig. 12, the output voltage and current of the two VSCs are given separately for normal operating state with R_D=0.5Ω (case 1), critical condition with R_D=370Ω (case 2) and unstable state with R_D=375Ω (case 3). It can be observed that the system can keep stable both for R_D=0.5Ω and R_D=370Ω, but there is a voltage drop when R_D=370Ω. On the other hand, the system loses stability when R_D is increased to 375Ω (case 3). During the experiments, the stability of the system plays randomly around 370 Ω - 375 Ω. It also reveals that the system goes near to the boundary. Based on (28) or (29), the operating angle limit

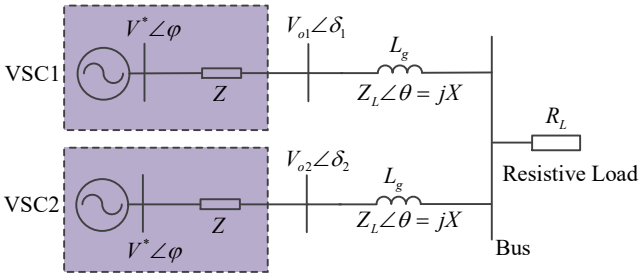

Fig. 11. The diagram of the experiment system.

can be estimated as $\delta_{\max} \ll 1°$. In this critical situation, a small disturbance even may lead the system to operate outside the feasible set and make VSCs lose the stability suddenly, which finally may lead the entire system to collapse. Since the inner current control loop has the fastest dynamic to face the situation, the output currents are distorted severely in the critical stable state (case 2, case 4 and case 5) and collapse first to draw the whole system down (case 3). Though there is an obvious voltage drop in the experiment, this instability phenomenon can be mainly treated as angle stability problem. In traditional electrical systems, voltage stability is usually regarded as a dynamic phenomenon driven by the loads. Obviously, the evolution of a real system can be more complex such that the system can lose the stability through different trajectory or path.

The above analysis and experiment reveal that the VSC's output impedance and line impedance influence the angle stability. When VSCs are operated in a weak network or there is a fault in the system, the equivalent line impedance (the electrical distance) of the network may change seriously. It may lead to the power curve shrink severely as is given in Fig. 9, which may lead to the operating points outside the feasible set for constant power loads (or consumption). Meanwhile, it should be recognized that most instability phenomenon in power systems are related to a fault or disturbance in emergency states.

However, as a corrective action, the system stability can be improved by increasing the given reference during the critical condition. The conclusion is verified by case 4 (both transient state and critical stable state) in Fig. 13, which are performed by increasing the given voltage reference V^* from 311 V to 1400 V. It shows that the control system and the DC side are decoupled in case of constant DC voltage, and the stability can be improved by increasing the output settings. It is an inverse process of the shrinking action in Fig. 9. The above experiments are based on a sufficient DC input power source (10 kW can be provided at most). If the stability of DC side can not be ensured in the critical condition, the system stability may decrease further as is given in equation (37). In this situation, DC side may lose stability in advance of the control system. In a VSC-based system, VSCs should have some additional active/reactive power margins in response to load increasing over the system capability. Furthermore, it is critical important for VSCs to keep the stability of DC side (with constant DC voltage) so that the AC system can be decoupled with the DC side as much as possible. These are part of the reasons that the

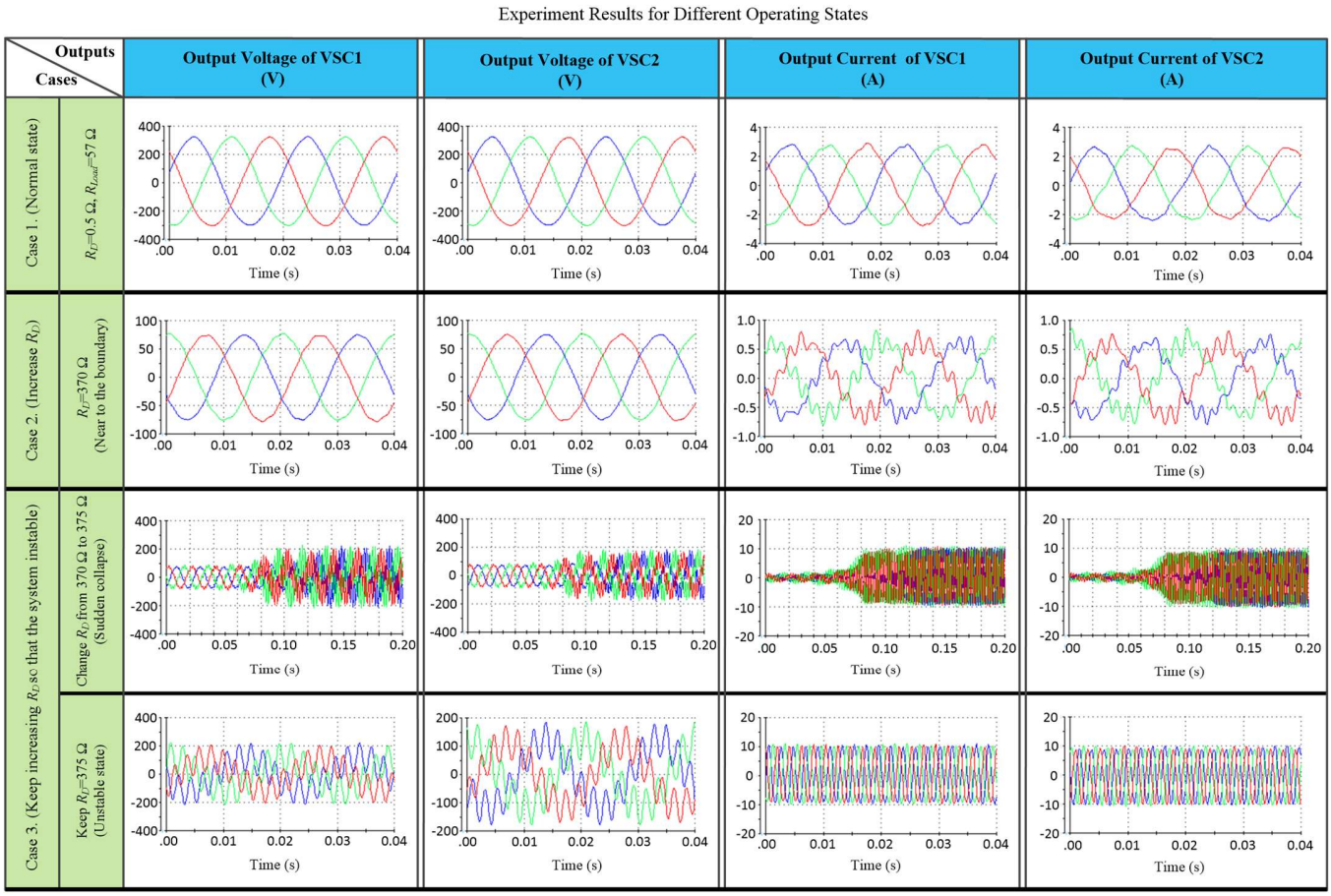

Fig. 12. The experiment results for different operating states.

stability of some renewable energy based VSCs play weakly in a real electrical system, e.g. photovoltaic units and wind turbines that operated in a maximum power output mode. As increasing the VSCs' output settings may result in a cheat that all reserves are going to be exhausted at the same time, it requires a more conservative and faster as well as coordinated "boosting" control (and also control center) at the emergency situations in a real system.

As another countermeasure, load shedding can also help increase the system margin that is verified by case 5 (Fig. 13). In this test, the loading is decreased (R_{Load} is increased) from 57Ω to 230 Ω then repeat the processing in case 4. Because the consumed active power becomes less, the margin/distance of the operating point is relatively lager from the limit $P_{\max}$ (and $\delta_{\max}$ etc.) so that the system can recover to critical stable state very fast with a smaller V^* value (550 V).

B. Further Discussion

The above theoretical analysis and experimental results illustrate that there is a feasible set of values limiting the entire system stable operation. The resulting boundary of this feasible set is a hyperplane due to the severe nonlinearities. So far, this perspective has not been clearly addressed in previous works that deal with the stability analysis in power electronics systems. Furthermore, the control scheme is a subsystem of the entire electrical system. If the system operating point is already beyond the feasible set of values, the whole system may lose stability even though the control sub-system is stable.

In case 3 of Fig. 12, the experimental results show that the system loses stability when R_D is increased to about 375 Ω with a feasible set much less than 1°. Though the feasible set is not reduced to 0, the system is still unstable because there are small disturbances, which cannot be avoid in dynamical systems, leading to the operating point outside the set and VSCs go to the unstable region.

Here, we give another simple case to explain/illustrate the stability analysis for VSCs supplying the constant power loads. As an instance given in Fig. 9, if the power curve is shrunk from curve 1 to curve 2 suddenly for some reasons (for example the network changes the topology), the system may lose stability for constant power consumption P_s even though the control system of VSCs may be stable at the current time, because the operating point has already been outside the feasible set. This is a simple but practical case for VSCs in electrical systems which contain lots of nonlinear loads such as constant power loads. Whereas, the methodology used in the previous literatures of power electronics system cannot explain this phenomenon very well for VSCs.

Therefore, the boundary of the feasible set is significant to understand and to avoid instability, since it gives a physical limit for the whole system. When we have known the margin or distance from the boundary, we can do some proper countermeasures to increase the system stability. It is also the

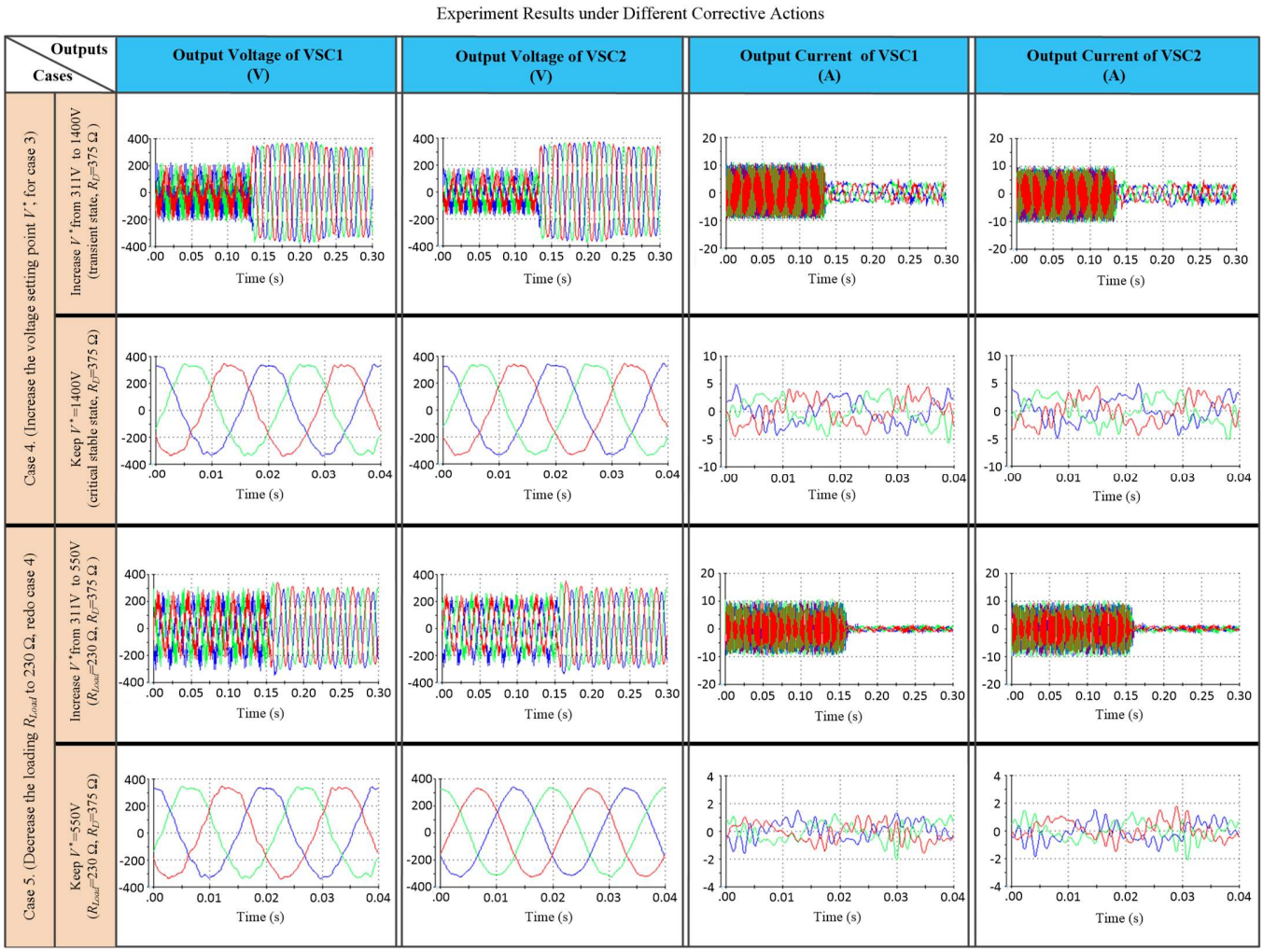

Fig. 13. The experiment results for different corrective actions.

contribution and motivation of this paper to reveal the angle instability phenomenon and propose a different stability analysis methodology. As is mentioned in Section III, this paper uses time scale decomposition perspective to get the approximated limitation (37) for angle stability analysis, which is only the necessary condition of the practical restriction. Even though (37) is not the exact limitation, with a proper simplification, it can give us an estimated safe margin or distance for the system operating point.

The experimental results of case 4 in Fig. 13 show that increasing the output level of the voltage sources is helpful for the system stability, since it increases the feasible set and the boundary, as well as the margin for the operating point. Once we can increase the number of voltage sources interconnected in a system at the same time without losing stability, it is may be a useful method for system operators. Of course, it must be performed in a reasonable and limited level in the real system, together with other optional countermeasures, such as loading shedding in the experiment test.

The transient instability of VSCs, under serious disturbances, can be simply viewed as the operating point located (suddenly) outside the current feasible set O in the power space which leads to the controller of VSCs lose stability or the DC-link side collapse. Due to the specific physical features of VSCs, the time scale of the transient instability process of VSCs may be much faster than synchronous generators, e.g. VSCs can lose stability directly without the apparent swings phenomenon that often happens in synchronous generators. Furthermore, there may be oscillation phenomenon on DC-link side and (or) AC side, when VSCs face some significant disturbances. Corrective actions can be regarded as the countermeasures of attracting the operating point back within the new feasible set O'. The saturation limiter in the controller, enhanced DC chopper circuit and storage unit can be adopted to limit the DC voltage deviation for VSCs, while shunt/series compensation, system protection and control schemes, and generator/load shedding are usually considered in utilities to face the contingencies.

VI. Conclusion

In this paper, the quasi-steady angle instability mechanism of voltage-controlled converters was first explained with mathematical deduction from the perspective of time scale decomposition. Meanwhile, the stability of DC-link side is deduced separately for constant DC voltage and constant DC input power. When the DC side voltage is constant, VSCs can

have the same angle stability criterion as synchronous generators, with various well designed control schemes. The experiment results with the corrective actions verify the analysis.

APPENDIX

Some additional explanation of the content is given in the appendix for further reading.

1. The equations of A_1, B and A_2 in equation (12) with the parameters of the system are:

$$A_1 = \left(-L\omega^2 - \omega^2 K_m k k_p L_D + K_m k k_i R_D\right)\left(K_m k k_i - \left(r + K_m k\right)C\omega^2\right) + \omega^2\left(r + K_m k + K_m k k_p R_D + K_m k k_i L_D\right)\left[K_m k k_p + 1 - LC\omega^2\right] \quad (40)$$

$$B = [K_m k k_i - (r + K_m k)C\omega^2]^2 + [(K_m k k_p + 1)\omega - LC\omega^3]^2 \quad (41)$$

$$A_2 = -\omega\left(-L\omega^2 - \omega^2 K_m k k_p L_D + K_m k k_i R_D\right)\left[K_m k k_p + 1 - LC\omega^2\right] + \omega\left(r + K_m k + K_m k k_p R_D + K_m k k_i L_D\right)\left(K_m k k_i - \left(r + K_m k\right)C\omega^2\right) \quad (42)$$

2. Small disturbance analysis of a dynamical system.

We define a dynamical system is as below:

$$\dot{x} = \frac{dx}{dt} = f(x) \quad (43)$$

Assume $x^*$is an equilibrium point so that $f(x^*) = 0$. Δx is a small disturbance around the equilibrium point x^*. For small disturbance analysis, the Taylor expansion of the dynamical system on $x^*+\Delta x$ is as following:

$$f(x^* + \Delta x) = f(x^*) + DF(x^*)\cdot\Delta x + O(\Delta x) \quad (44)$$

where

$$DF(x) = \begin{bmatrix} \frac{\partial f_1}{\partial x_1} & \cdots & \frac{\partial f_1}{\partial x_n} \\ \vdots & \ddots & \vdots \\ \frac{\partial f_n}{\partial x_1} & \cdots & \frac{\partial f_n}{\partial x_n} \end{bmatrix}$$

$DF(x^*)$ is the partial derivative of $f(x)$ on x^*, which is usually called Jacobian matrix. $O(\Delta x)$ is the high order terms with respect to Δx, which can be ignored in the analysis.

Because $f(x^*) = 0$, we have:

$$\Delta\dot{x} = DF(x^*)\cdot\Delta x \quad (45)$$

The above differential equation with respect to Δx can be solved as:

$$\Delta x(t) = \sum_{i=1}^{N} A_i\vec{e}_i \cdot \exp(s_i t) \quad (46)$$

where s_i is the eigenvalue of $DF(x^*)$, and the initial value of $\Delta x(0) = \sum_{i=1}^{N} A_i\vec{e}_i$.

If all eigenvalues of $DF(x^*)$ have negative real parts, the dynamical system $\dot{x} = f(x)$ is stable on x^*, because the small disturbance $\Delta x(t) = \sum_{i=1}^{N} A_i\vec{e}_i \cdot \exp(s_i t)$ keeps decreasing.

If at least one eigenvalue of $DF(x^*)$ has the positive real part, the system is instable, because the small disturbance $\Delta x(t) = \sum_{i=1}^{N} A_i\vec{e}_i \cdot \exp(s_i t)$ keeps increasing toward certain directions.

If there are a pair of eigenvalues in $DF(x^*)$ having 0 real part or one eigenvalue equaling to 0, the system is operated in critical stabile state. The system may lose the stability with periodic oscillations.

The above eigenvalues analysis is valid for both time and frequency domain system. Comparing with frequency domain methods that is widely used in power electronics system, time domain analysis has the advantage of revealing the exact evolution of a dynamical system more intuitively though it is relatively difficult on calculation. Therefore, the author actually combines both frequency domain and time domain analysis as a contribution in the paper. The frequency domain method is mainly used to design the reasonable parameters to ensure the control system work well, while the time domain method is adopted for stability analysis to reveal the instability mechanism. In this paper, for simplifying the analysis, the author assumes the transient dynamics of VSCs are infinitely fast and stable from a time scale decomposition perspective. In power industry, however, the real-time calculation can be improved for an entire complex dynamical system based on the numerical calculation in modern computers.

REFERENCES

[1] Holmes D G, Lipo T A, McGrath B P, "Optimized design of stationary frame three phase AC current regulators," *IEEE Trans. Power Electron*., vol. 24, no. 11, pp. 2417-2426, Nov. 2009.

[2] Zmood D N, Holmes D G, "Stationary frame current regulation of PWM inverters with zero steady-state error," *IEEE Trans. Power Electron*., vol. 18, no.3, pp.814-822, May 2003.

[3] Zmood D N, Holmes D G, Bode G H, "Frequency-domain analysis of three-phase linear current regulators," *IEEE Trans. Ind. Appl*., vol.37, no. 2, pp. 601-610, Mar./Apr. 2001.

[4] S. Jian, "Impedance-based stability criterion for grid-connected inverters," *IEEE Trans. Power Electron.,* vol. 26, no. 11, pp. 3075–3078, Nov. 2011.

[5] J. H. R. Enslin and P. J.M. Heskes, "Harmonic interaction between a large number of distributed power inverters and the distribution network," *IEEE Trans. Power Electron*., vol. 19, no. 6, pp. 1586–1593, Nov. 2004.

[6] M. Liserre, R. Teodorescu, and F. Blaabjerg, "Stability of photovoltaic and wind turbine grid-connected inverters for a large set of grid impedance values," *IEEE Trans. Power Electron*., vol. 21, no. 1, pp. 263–272, Jan. 2006.

[7] M. Cespedes and S. Jian, "Renewable energy systems instability involving grid-parallel inverters," in *Proc. 24th Annu. Appl. Power Electron. Conf. Expo.*, Mar. 2009, pp. 1971–1977.

[8] E. Vittal, M. O'Malley, and A. Keane, "A steady-state voltage stability analysis of power systems with high penetrations of wind," *IEEE Trans. Power Syst.*, vol. 25, no. 1, pp. 433–442, Feb. 2010.

[9] L. Harnefors, M. Bongiorno, and S. Lundberg, "Input-admittance calculation and shaping for controlled voltage-source converters," *IEEE Trans. Ind. Electron.*, vol. 54, no. 6, pp. 3323–3334, Dec. 2007.

[10] M. Cespedes and S. Jian, "Impedance shaping of three-phase grid-parallel voltage-source converters," *in Proc. 27th Annu. Appl. Power Electron. Conf. Expo.,* Mar. 2012, pp. 754–760.

[11] K. M. Alawasa, Y. A. R. I. Mohamed, and W. Xu, "Modeling, analysis, and suppression of the impact of full-scale wind-power converters on subsynchronous damping," *IEEE Syst. J*., vol. 7, no. 4, pp. 700–712, Dec. 2013.

[12] Alawasa K M, Mohamed Y A R I, Xu W, "Active mitigation of subsynchronous interactions between PWM voltage-source converters

and power networks," *IEEE Trans. Power Electron*., vol. 29, no. 1, Jan. 2014.
[13] O. Mo, M. Hernes, and K. Ljokelsoy, "Active damping of osicllations in LC-filter for line connected, current controlled, PWM voltage source converters," *in Proc. Eur. Conf. Power Electron*., 2003, pp. 1–10.
[14] M. Schweizer and J. W. Kolar, "Shifting input filter resonances—An intelligent converter behavior for maintaining system stability," *in Proc. IEEE Int. Power Electron. Conf*., 2010, pp. 906–913.
[15] K. M. Alawasa, Y. A. R. I. Mohamed, and W. Xu, "Active mitigation of subsynchronous interactions between PWM voltage-source converters and power networks," *IEEE Trans. Power Electron.,* vol. 29, no. 1, pp. 121–134, Jan. 2014.
[16] Wen B, Boroyevich D, Burgos R, "Analysis of dq small-signal impedance of grid-tied inverters," *IEEE Trans. Power Electron*., vol. 31, no. 1, pp. 675-687, Jan. 2016.
[17] Wen B, Boroyevich D, Burgos R, "Small-signal stability analysis of three-phase ac systems in the presence of constant power loads based on measured dq frame impedances," *IEEE Trans. Power Electron*., vol. 30, no. 10, pp. 5952-5963, Oct. 2015.
[18] Rokrok E, Golshan M E H, "Adaptive voltage droop scheme for voltage source converters in an islanded multibus microgrid," *Generation, Transmission & Distribution, IET*, vol. 4, no. 5, pp. 562-578, Jan. 2010.
[19] Lee C T, Chu C C, Cheng P T, "A new droop control method for the autonomous operation of distributed energy resource interface converters," *IEEE Trans. Power Electron*., vol. 28, no. 4, pp. 1980-1993, Apr. 2013.
[20] Díaz G, Gonzalez-Moran C, "Gomez-Aleixandre J, et al. Scheduling of droop coefficients for frequency and voltage regulation in isolated microgrids," *IEEE Trans. Power Syst.*, vol. 25, no.1, pp. 489-496. Feb. 2010.
[21] Coelho E A A, Cortizo P C, Garcia P F D. "Small-signal stability for parallel-connected inverters in stand-alone AC supply systems," *IEEE Trans. Ind. Appl*., vol. 38, no. 2, pp. 533-542. 2002.
[22] Guerrero J M, Vicuña D, García L, "A wireless controller to enhance dynamic performance of parallel inverters in distributed generation systems," *IEEE Trans. Power Electron.*, vol. 19, no. 5, pp. 1205-1213, 2004.
[23] Guerrero J M, Vicuña D, García L, "Output impedance design of parallel-connected UPS inverters with wireless load-sharing control," *IEEE Trans. Ind. Electron*., vol. 52, no.4, pp. 1126-1135, 2005.
[24] U. Borup, F. Blaabjerg, and P. Enjeti, "Sharing of nonlinear load in parallel connected three-phase converters," *IEEE Trans. Ind. Appl*., vol. 37, no. 6, pp. 1817–1823, Nov./Dec. 2001.
[25] Guerrero J M. Castilla, L. G. Vicuna, J. Miret, and J. Vasquez, "Virtual impedance loop for droop-controlled single-phase parallel inverters using a second-order general-integrator scheme," *IEEE Trans. Power Electron*., vol. 25, no. 12, pp. 2993–3002, Dec. 2010.
[26] R. D. Middlebrook, "Input filter considerations in design and application of switching regulators," *in Proc. IEEE Ind. Appl. Soc. Conf*., Oct. 1976, pp. 94–107.
[27] Q.-C. Zhong and G. Weiss, "Synchronverters: Inverters that mimic synchronous generators," *IEEE Trans. Ind. Electron*., vol. 58, no. 4, pp. 1259–1267, Apr. 2011.
[28] T. Shintai, Y. Miura, and T. Ise, "Oscillation damping of a distributed generator using a virtual synchronous generator*," IEEE Trans. Power Del.,* vol. 29, no. 2, pp. 668–676, Apr. 2014.
[29] Y. Hirase, O. Noro, E. Yoshimura, H. Nakagawa, K. Sakimoto, and Y. Shindo, "Virtual synchronous generator control with double decoupled synchronous reference frame for single-phase inverter," *in Proc. Int. Power Electron. Conf.,* 2014, pp. 1552–1559.
[30] Y. Chen, R. Hesse, D. Turschner, and H.-P. Beck, "Improving the grid power quality using virtual synchronous machines," *in Proc. Int. Conf. Power Eng. Energy. Elect. Drives*, 2011, pp. 1–6.
[31] Akhrif O, Okou F A, Dessaint L, "Application of a multivariable feedback linearization scheme for rotor angle stability and voltage regulation of power systems," *IEEE Trans. Power Syst.*, vol. 14, no. 2, pp. 620-628. May 1999.
[32] Prabha Kundur, *Power system stability and control*, New York, USA: McGraw-hill, 1994.
[33] P. W. Sauer and M. A. Pai, *Power Systems Dynamics and Stability*. Englewood Cliffs, NJ: Prentice-Hall, 1997.

Hengwei Lin (S'14–M'17) received the B.S. degree in electrical engineering, the M.S. degree in power electronics and motor drives from Yanshan University, Qinhuangdao, China, in 2010 and 2013, respectively, and Ph.D. degree in Energy Technology from Aalborg University, Aalborg, Denmark, in 2017.

From June 2016 to September 2016, he was a Visiting Scholar at Argonne National Laboratory, Chicago, IL, USA. His research interests are stability and control in electrical systems, protection in microgrids and renewable energy systems, and machine learning.

Chenxi Jia (S'17) was born in Shijiazhuang, China. She received the B.S. degree in electrical engineering from Yanshan University, Qinhuangdao, China, in 2013, and the M.S. degree in electrical engineering from Beijing Jiaotong University, Beijing, China, in 2016.

Her research interests are power electronics and motor drives, renewable energy systems, and machine learning.

Josep M. Guerrero (S'01-M'04-SM'08-FM'15) received the B.S. degree in telecommunications engineering, the M.S. degree in electronics engineering, and the Ph.D. degree in power electronics from the Technical University of Catalonia, Barcelona, in 1997, 2000 and 2003, respectively. Since 2011, he has been a Full Professor with the Department of Energy Technology, Aalborg University, Denmark, where he is responsible for the Microgrid Research Program (www.microgrids.et.aau.dk).

His research interests are oriented to different microgrid aspects, including power electronics, distributed energy-storage systems, hierarchical and cooperative control, energy management systems, smart metering and the internet of things for AC/DC microgrid clusters and islanded minigrids; recently specially focused on maritime microgrids for electrical ships, vessels, ferries and seaports. Prof. Guerrero is an Associate Editor for the IEEE TRANSACTIONS ON POWER ELECTRONICS, the IEEE TRANSACTIONS ON INDUSTRIAL ELECTRONICS, and the IEEE Industrial Electronics Magazine, and an Editor for the IEEE TRANSACTIONS on SMART GRID.

Juan C. Vasquez (M'12-SM'14) received the B.S. degree in electronics engineering from the Autonomous University of Manizales, Manizales, Colombia, and the Ph.D. degree in automatic control, robotics, and computer vision from the Technical University of Catalonia, Barcelona, Spain, in 2004 and 2009, respectively. In 2011, he was Assistant Professor and from 2014 he is working as an Associate Professor at the Department of Energy Technology, Aalborg University, Denmark where he is the Vice Programme Leader of the Microgrids Research Program. His current research interests include operation, advanced hierarchical and cooperative control and the integration of Internet of Things into the SmartGrid.

Dr. Vasquez is currently a member of the IEC System Evaluation Group SEG4 on LVDC Distribution and Safety for use in Developed and Developing Economies, the Renewable Energy Systems Technical Committee TC-RES in IEEE Industrial Electronics, PELS, IAS, and PES Societies.